A REVIEW OF VACUUM-ARC MULTILAYER COATINGS WITH HIGH-STRENGTH CHARACTERISTICS AND ADHESIVE PROPERTIES

O.V. Maksakova[a,b], S.V. Lytovchenko[a]*, V.M. Beresnev[a], S.A. Klymenko[c], D.V. Horokh[a], B.O. Mazilin[a], M.Y. Kopeykina[c], S.An. Klymenko[c], V.V. Grudnitskii[d], O.V. Gluhov[e], R.S. Galushkov[a]

[a]V.N. Karazin Kharkiv National University, 4, Svoboby Sq., 61000 Kharkiv, Ukraine
[b]Institute of Materials Science, Slovak University of Technology in Bratislava, 25, Jána Bottu Str., 917 24 Trnava, Slovakia
[c]Bakul Institute for Superhard Materials, National Academy of Sciences of Ukraine, 2, Avtozavodskaya Str, Kyiv, 04074, Ukraine
[d]National Science Center "Kharkov Institute of Physics and Technology", 1, Akademicheskaya St, Kharkiv, 61108, Ukraine
[e]Kharkiv National University of Radio Electronics, Nauky Ave. 14, Kharkiv, 61166, Ukraine
*Corresponding Author e-mail: s.lytovchenko@karazin.ua
Received August 22, revised October 21, 2024; accepted November 12, 2024

Using the TiSiN/MeN (Me = Cr, Nb, W, Mo, TiZr) coatings system as an example, the analyzed results of multilayer coatings with nanolayers of various functional purposes require a systematic approach to understanding the role of selected materials, growth conditions, microstructure, and required properties. Nanoscale grain boundaries, coherent interlayer boundaries, and changes in columnar morphology at the micro level significantly change the physical and mechanical properties of coatings. For all coatings, an increase in mechanical parameters (hardness, modulus of elasticity) is observed due to the formation of a nanoscale phase (which additionally prevents the movement of dislocations together with nanocomposite TiSiN). In addition, there is a mismatch of crystal lattices between layers. Effectively contributes to strengthening due to variable fields of stresses and strains caused by deformations of elastic coherence. Research has determined optimal conditions for the formation of coatings in a wide range of gas (nitrogen) pressure and shear potential, which also allowed for establishing the factors of structural changes and operational characteristics that will be optimal for their industrial use.

Key words: *Cathodic vacuum arc physical vapor deposition; Multilayer coatings; TiSiN; Bias potential; Hardness; Phase state; Annealing*
PACS: 68.55.Jk, 68.65.Ac

INTRODUCTION

A complex of structural materials with enhanced physical and mechanical properties is used to improve the reliability and durability of modern technology in operation. However, to increase the performance of products, in particular cutting tools, it is relevant to create and use protective coatings, whose principle is based on a complex of tribological and mechanochemical effects that determine the ability of coatings to maintain their integrity and high wear resistance under the influence of high temperatures and contact loads [1-3]. One of the key trends in developing these coatings is to ensure the nanoscale of both structural elements and individual layers in multilayer compositions [4-8]. The formation of the nanoscale structure of the coating materials is related to the choice of graininess, which is optimal according to the strength criterion, the balance between the Hall-Patch dependence, and the expression that determines the rate of grain boundary creep with decreasing grain size. The efficiency of applying such coatings is attributed to the combination of their high physical and mechanical properties, resistance to oxidation, and dissociation of the chemical compounds included in their composition due to the peculiarities of the structure of nanocomposite film systems. Immersing nanocrystalline grains in the amorphous matrix of the second phase of the material, for example, Si_3N_4 can boost the physical and mechanical properties of TiN coatings, increasing their oxidation resistance and thermal stability [9, 10].

In work [11], it was found that the process of destruction of TiSiN nanocomposite coatings changed from brittle to ductile when the residual compressive stress decreased to the level at which the microcracks were activated. The residual stress of deposited coatings consists of three parts: the epitaxial or structural mismatch between the seed film and the substrate, the internal stress, and the thermal stress during the post-coating cooling process. Annealing is a common method of reducing residual stress as a result of reducing defects, dislocations, and vacancies [12]. However, this treatment also reduces the hardness of coatings obtained by ion bombardment [13].

For this reason, developing TiSiN coatings with a multilayer architecture is considered a more effective method to improve viscosity and wear resistance, reduce residual stress, and maintaining high hardness [4].

First and foremost, the lattice mismatch and the interface between the different layers can cause the lattice to distort to accommodate the applied stress and create an alternating stress field to reduce the stress concentration. Additionally, different stress properties in each coating can reduce overall stress [14].

In work [15], the wear behavior and adhesive properties of multilayer MeN/TiSiN (Me = Ti, Cr, Zr, Mo, Nb_xAl_{1-x}) coatings with variable second layers were studied. Multilayer coatings based on TiSiN alternated with TiN, ZrN, NbAlN, CrN, and MoN with a fixed number of layers were synthesized by cathodic arc ion sputtering. Multilayer coatings based on TiSiN exhibit a precise nanocomposite multilayer structure. Columnar grains are not observed because the growth of crystalline nitride grains is blocked by amorphous Si_3N_4 or interfaces. High adhesion (with a critical load of more than 70 N) and a lower coefficient of friction (between 0.3 and 0.58) are achieved for all multilayer coatings.

In work [16], the investigation of multilayer coatings of the TiSiN/CrN system by cathodic arc evaporation with different multilayer periods (Λ) of 8.3 nm, 6.2 nm, and 4.2 nm was reported. It revealed the formation of a typical columnar structure and B1-NaCl crystalline with a maximum hardness of 37±2 GPa and the lowest wear rate of 0.323 GPa for the coating with Λ = 8.3 nm. This suggests that the mechanical and tribological properties of TiSiN-based coatings can be enhanced through the design of multilayer coatings.

To enhance the oxidation and/or mechanical properties of TiSiN-based coatings, intensive efforts have been made to explore multilayer structures. In work [17], nano-multilayer TiSiN/TiAlN films were reported by a dual cathodic arc plasma evaporation system with a hardness ranging from 32 to 38 GPa. The potentiodynamic polarization measurements showed that for all the multilayered coatings the corrosion potential shifted to higher values, and the corrosion current density decreased, indicating better corrosion resistance than that of single-layer coatings like TiAlN or TiSiN [18-20].

According to this principle, TiSiN-based multilayer coatings have attracted a great deal of interest. The existing literature shows that most scientific researchers focus on the influence of the bilayer period on the microstructure and mechanical properties of TiSiN-based multilayer coatings. However, there are relatively few studies devoted to the investigation of the properties, which is the most important factor for the application.

To summarise data on TiSiN-based multilayers for specific applications, we decided to write this review paper, which concludes the results of newly published experiments on multilayer coatings TiSiN/MeN (Me = Cr, Nb, W, Mo, and TiZr).

MATERIAL AND METHODS

The architectural solution of composite multilayer coatings based on TiSiN is presented in Figure 1.

Multilayer coating systems TiSiN/MeN (Me = Cr, Nb, W, Mo, and TiZr) were synthesized by cathodic vacuum arc physical vapor deposition (CVA-PVD). The scheme of the cathodic-arc deposition machine is depicted in Figure 2.

Two evaporators were used to obtain TiSiN/MeN coatings. The cathodes were sintered from the TiSi target (chemical specification in at. % is $Ti_{94}Si_6$) and Me targets such as Cr, Nb, W, Mo (purity specification is 99.8 %) and sintered TiZr (chemical specification in at. % is $Ti_{75}Zr_{25}$). Nitrogen was supplied by injecting N_2 gas (a purity of 99.6 %) into the deposition chamber.

The coating systems were deposited on stainless steel (grade 12X18H9T or an analogue of SUS321 and 321S51) with dimensions of 20 mm×20 mm×2 mm.

The specific technological parameters during the deposition of multilayer coatings are summarized in Table 1.
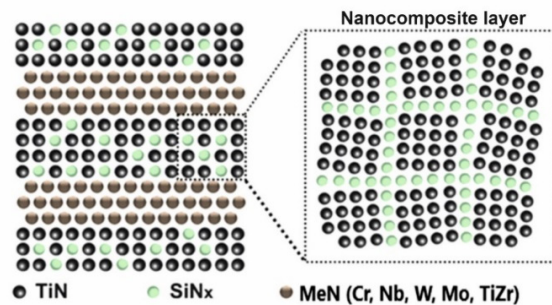
Figure 1. The architecture scheme of composite multilayer coating systems TiSiN/MeN (Me = Cr, Nb, W, Mo, and TiZr).
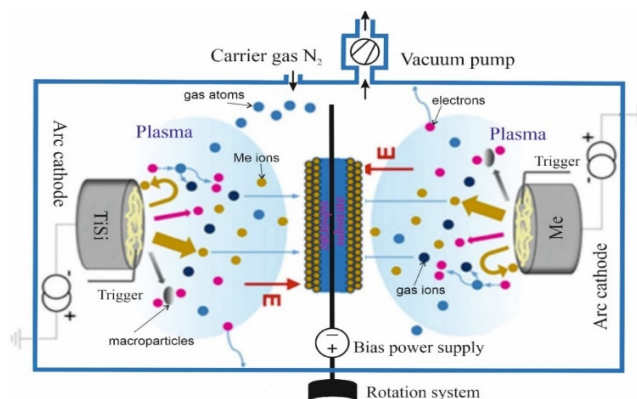
Figure 2. Scheme of the CAE-PVD machine used for the deposition of the multilayer coating systems TiSiN/MeN (Me = Cr, Nb, W, Mo, and TiZr). Adapted from [21].

Table 1. Deposition parameters of multilayer coating systems TiSiN/MeN (Cr, Nb, W, Mo, and TiZr).

Coating	Sample no.	Arc current, A	Negative bias, V	Gas pressure, Pa	Coating thickness, μm	Multilayer period, nm
TiSiN/ CrN	1	110/90	-100	0.08	7-10	6.7-12.5
	2			0.3		
	3			0.06		
	4	110/80	-200	0.08		
	5			0.3		
	6			0.6		
TiSiN/NbN	1	110/80	-110	0.53	5.1	56
	2		-200		4.5	50
	3		-110	0.13	6.8	75
	4		-200		6.3	70
TiSiN/WN	1	100	-200	0.6	4.2	10.5
TiSiN/TiZrN	1	80-85	-200	0.6	3.61	40.1
	2			0.13	3.72	40.9
	3			0,6	3.67	20.4
	4				3.96	85.9
TiSiN/MoN	1	140/100	-100	0.05	9-11	7-8
	2		-200			
	3	140/100	-100	0.13		
	4		-200			
	5	140/100	-100	0.67		
	6		-200			

DISCUSSIONS
Coatings of TiSiN/NbN system

Experimental results for multilayer TiSiN/NbN coatings are shown in Figure 3 and Figure 4 and adopted from [21-23]. The TiSi target was obtained by the vacuum-arc remelting method. The composition of targets was $Ti_{94}Si_6$ and $Nb_{99.8}$. As can be seen, the surface morphology of the coatings has a well-defined cellular structure (Figure 3, left panel). There are many shallow craters with a diameter of 0.3 to 5 μm. Solid inclusions in the form of drops are unevenly distributed over the surface and occupy approximately 15 % of the surface area. The diameter of the droplets varies between 2 to 10 nm.

In the cross-section, the coatings are evenly deposited on the substrate and have a dense structure. A clear periodic arrangement of nanoscale layers in the laminar architecture is observed (Figure 3, right panel). The thickness of the NbN layers is 20 % greater than the thickness of the TiSiN layers. This difference in thickness can be attributed to a lower rate of evaporation of the TiSi cathode, which mainly consists of the refractory intermetallic compound $TiSi_2$, compared to pure niobium. Additionally, the smaller thickness and higher density of TiSiN can also be explained by the lower formation energy of TiSiN compared to NbN. The structure of the NbN layers is more difficult to densify by ion bombardment, which is generated by the -110 V and -200 V bias voltages applied to the substrate during coating production. Thus, both phenomena lead to the formation of thinner but denser TiSiN layers. According to elemental analysis data, it was established that the coatings obtained at a higher bias potential of -200 V have a lower concentration of Si ranging between 0.8 to1.0 at. % than the coatings obtained at a lower bias potential of -110 V.

According to XRD patterns (see Figure 4a), it was established that in the coatings obtained at low values of the bias potential of -110 V (samples nos. 1 and 3), two phases are formed: face-centered cubic (fcc) titanium nitride TiN (space group No. 225) and hexagonal close-packed (fcc) niobium nitride NbN-δ' (space group No. 194). Analysis of the intensity and position of the peaks indicates the presence of a (111) texture in fcc-TiN and a strong (00.2) texture in hcp-NbN-δ' for the coating obtained at a pressure of 0.13 Pa (sample no. 1). An increase in the gas pressure to 0.53 Pa leads to a redistribution of the peak intensity and a shift in their position, which indicates the practically non-textured state of the sample no. 3.

An increase in the negative bias potential leads to the appearance of clear high-intensity peaks in the diffraction patterns, which indicate the formation of a nanocrystalline state in the coatings (see Figure 4b). For the sample obtained at a low pressure of 0.13 Pa (sample no. 2), two phases are formed: fcc-TiN and hcp-bN-δ'. However, with an increase in pressure to 0.53 Pa, structural and phase transformations occur in the coatings, leading to the appearance of the third phase - face-centered cubic (fcc) niobium nitride NbN (space group No. 225) (sample no. 4). Due to the complex structure of the samples, the diffractogram has many diffraction planes for different phases, and some peaks overlap.
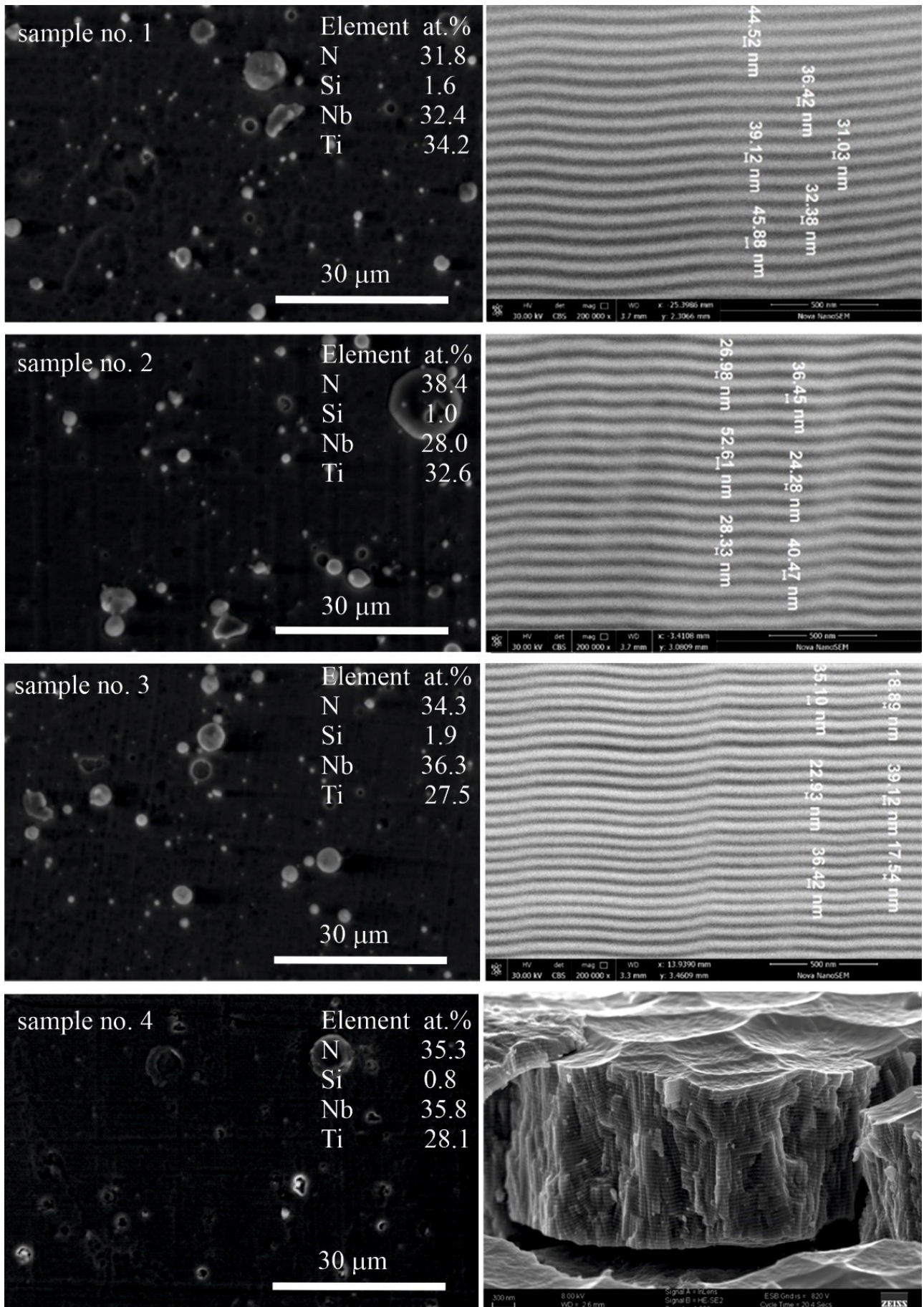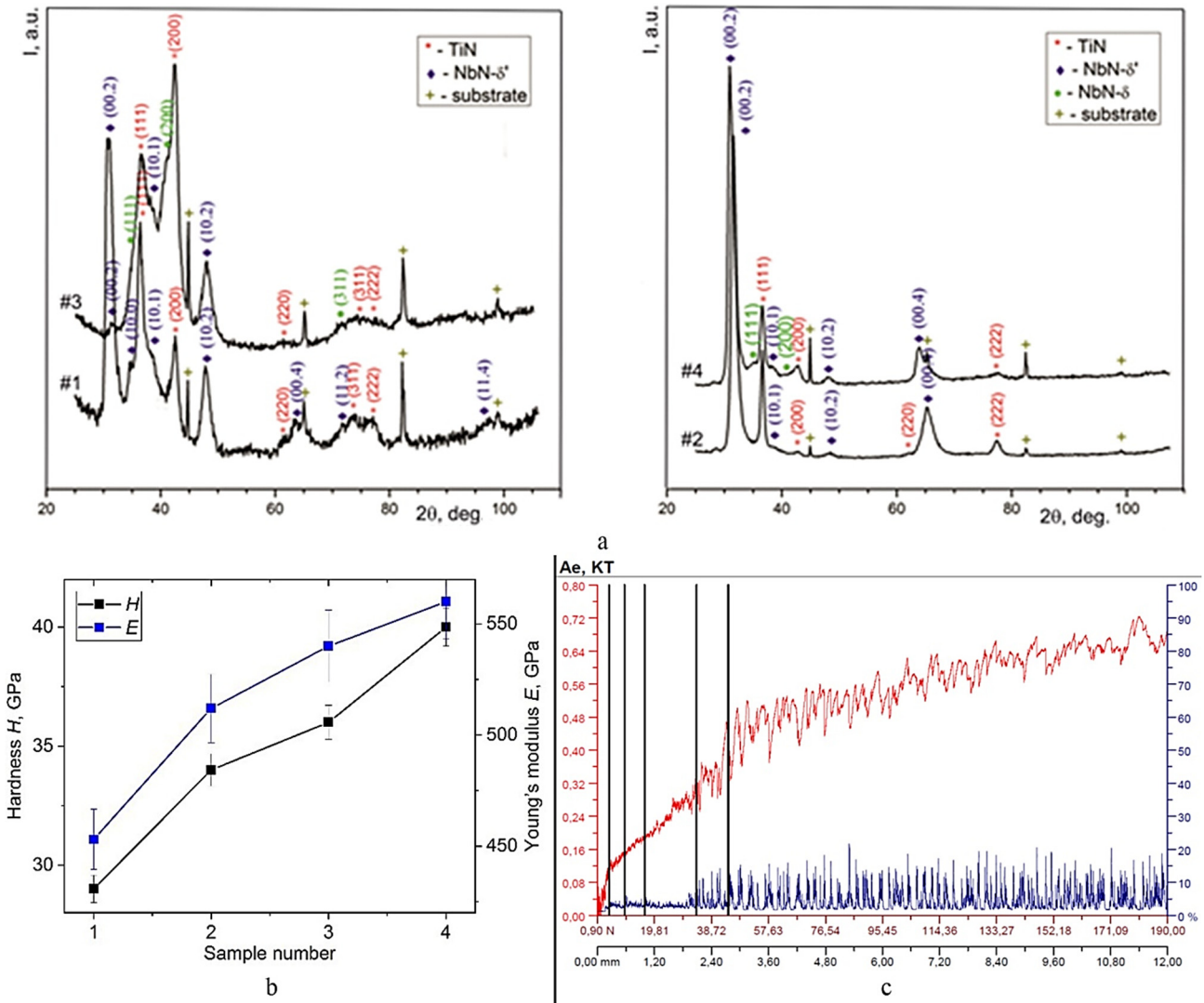
Figure 3. Scanning electron microscopy images of the surface and cross-section of multilayer coatings TiSiN/NbN.

Figure 4. General research results of multilayer coatings TiSiN/NbN: XRD patterns (*a*), Hardness and Young's modulus (*b*), results of sclerometric studies of the sample no. 2 (the red line corresponds to the friction coefficient (COF) and the blue line corresponds to the acoustic emission (AE)) (*c*).

The average grain size ranges from 8 to 14 nm. The lattice parameter for TiN ranges from 0.4250 to 0.4256 nm and is slightly increased compared to the reference fcc-TiN (a = 0.4240 nm according to JCPDS). This indicates the formation of residual compressive stresses in the coatings.

For TiSiN/NbN coatings, an increase in mechanical parameters is observed (see Figure 4b). The hardness grows up to 34.4 GPa, and the modulus of elasticity rises up to 412 GPa. This is due to the formation of a nano-sized NbN phase (which additionally prevents the movement of dislocations together with nanocomposite TiSiN). In addition, the crystal lattice mismatch between the TiSiN and NbN layers effectively contributes to strengthening due to variable stress and strain fields caused by elastic coherence deformations. The multilayer architecture contributes to the reduction of grain sizes and the increase of the volume fraction of atoms located at the interfaces of layers, thereby preventing the propagation of dislocations.

Adhesive strength tests (see Figure 4c) indicate a cohesive failure mechanism of TiSiN/NbN coatings, which is associated with plastic deformation and the formation of fatigue cracks in the material. The maximum load resulting in plastic abrasion of sample no. 2 is greater than 49.76 N, which indicates a high degree of strength of the coating and high adhesive properties of the contact between the coating and the substrate.

Coatings of TiSiN/CrN system

Figure 5 shows experimental results for multilayer TiSiN/CrN coatings adopted from [24, 25]. The vacuum-arc remelting method was applied to sinter the TiSi target. The composition of targets were $Ti_{94}Si_6$ and $Cr_{99.9}$. Since the TiSiN and CrN films have a face-centered cubic structure, in the multilayer architecture, which is depicted in Figure 5a, the TiSiN and CrN nanolayers tend to grow epitaxially, which will reduce the interfacial energy in the coatings. As the thickness of the CrN nanolayer increases, the increase in strain energy due to the different lattice parameters of TiSiN and

CrN disrupts the coherent interface. Thus, the structure of the epitaxial growth between TiSiN and CrN can be disturbed, which leads to a deterioration of crystallinity.

The elemental analysis results established that all TiSiN/CrN coatings have a slightly higher stoichiometric composition, confirmed by the ratio of metal elements to nitrogen (Ti + Si + Cr)/N (see Figure 5a, insert). The coating of sample no.3 obtained at the bias potential of -100 V and nitrogen pressure of 0.6 Pa has the maximum silicon concentration. As the bias potential increases to -200 V, the silicon concentration drops several times. Apparently, this is due to the preferential atomization of light silicon atoms from the surface of the growing coating due to ion bombardment. The higher the shear potential and the lower the gas pressure in the chamber, the stronger this effect.

The analysis of the secondary mass spectrometry is presented in Figure 5b. It confirms the presence of positive ions in the spectra, in particular Ti, Cr, Si (at 28–30 min with low intensity), TiN, CrN, Ti_2, TiCr, Ti_2N, Ti_2N_2 (probably TiSi in the case of the presence of a layer of TiSiN), as well as Ti_3N, $Ti_3(N_2)(Si)$, $Ti_3(N_3)(SiN)$. The spectrum of negative ions revealed the presence of SiN, TiN, and CNI(Cr, Cr_2), which shows a maximum at the beginning of the sputtering and decreases and reaches a plateau after 45–60 min. The intensity of the secondary ion current for TiN and Tix bonds is relatively small in the first five minutes of sputtering, then increases sharply, reaches a maximum, and soon (after 45-60 minutes) reaches a plateau.
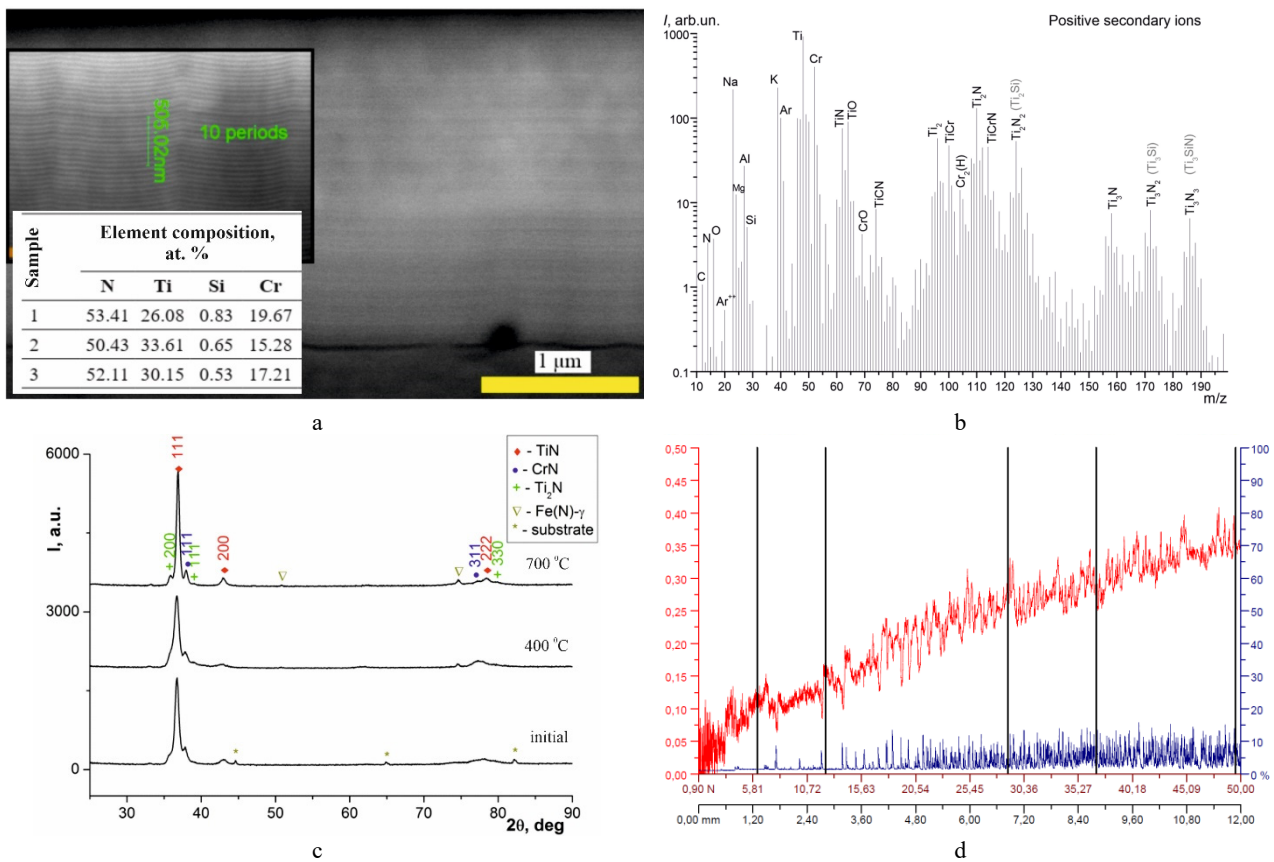
Figure 5. General research results of multilayer coatings TiSiN/CrN: typical SEM image of cross-section with chemical analysis for sample nos. 1-3 (a), spectrum of positive secondary ions for sample no. 3 (b), typical XRD patterns (c), results of sclerometric studies of the sample no. 3 (the red line corresponds to the friction coefficient (COF) and the blue line corresponds to the acoustic emission (AE)) (d)

X-ray patterns of multilayer TiSiN/CrN coatings in the initial state show the formation of three main nitride phases, in particular, face-centered cubic (fcc) TiN (JCPDS 38-1420) and Ti_2N phase (JCPDS 23-1455) with tetragonal (anti-) rutile type structure (space group P42/mnm) for TiSiN layers, and face-centered cubic (fcc) CrN (JCPDS 65-2899) for CrN layers (see Figure 5c). For these coatings, the Ti_2N phase leads to a high level of microdeformations with a value of 7.5×10^{-3}. The main crystalline phase is TiN with a cubic B1 (NaCl-type) structure. Applying a negative bias potential to the substrate during deposition leads to a highly textured state with a predominant orientation along the (111) axis. In addition, it increases the number of defects in the crystal structure and the level of residual compressive stresses.

After annealing the coatings at 400 °C (see Figure 5c), the phase composition TiSiN/CrN of sample no. 1 does not change. Still, crystallization occurs in the CrN layers, as indicated by separating the CrN(111) peak from the highly intensive TiN(111) peak. Increasing the annealing temperature to 700 °C also does not lead to a change in the phase composition of the coatings or the texture. Still, the separation of the CrN(111) peak becomes much more noticeable. At the same time, low-intensity peaks of $Ti_2N(200)$, $Ti_2N(111)$, $Ti2N(330)$, and CrN(311) appear. Annealing leads to a greater decrease in the lattice parameters of all phases by 2-3 % and a decrease in the level of microdeformations from

7.5×10^{-3} to 7.2×10^{-3}. After annealing at 700 °C (see Fig. 5c), the content of Si in the upper layers of the coatings increased due to intensive diffusion of silicon from the depth of the coating to the surface. At the same time, at 700 °C, a change in the stoichiometry of the coatings accompanies the annealing process. All coatings acquire a pre-stoichiometric composition as the concentration of N decreases from (50.43 ÷ 53.41) to (48.18 ÷ 49.16) at. %.

According to the mechanical tests, all TiSiN/CrN coatings are pretty hard (hardness values varied between 27.8 and 31.1 GPa) in the initial state. Annealing the coatings at 400 °C increases the hardness to (29.1 ÷ 32.8) GPa. A further increase in the annealing temperature to 700 °C slightly reduces the hardness of the coatings to the range of (28.8 ÷ 30.9) GPa. The coating sample no. 3, obtained at a bias potential of -200 V and a working gas pressure of 0.6 Pa, has the best mechanical properties both in the initial and after annealing. The coating hardness and elastic modulus have maximum values of 31.1 GPa and 298 GPa (32.8 GPa and 311 GPa at 400 °C and 30.9 GPa and 301 GPa at 700 °C), respectively. The higher hardness of this sample is due to the higher level of crystallinity of the TiSiN layers in the multilayer structure (according to the Pathscheider model). The H^3/E^2 values of the coatings are also exceptionally high both in the initial state (0.20 ÷ 0.33) and after annealing at 400 °C (0.23 ÷ 0.36) and at 700 °C (0.23 ÷ 0.32), which indicates their reasonably high resistance to mechanical loads without and under the influence of temperature.

The results of the adhesive tests, presented in Figure 5d, show that the coatings wear out under load, but do not peel off. Coating destruction occurs through a cohesive mechanism associated with plastic deformation and the formation of fatigue cracks in the coating material. It was found that the adhesive strength of TiSiN/CrN coatings obtained at a nitrogen pressure of 0.6 Pa and a bias potential of -100 B is higher by 10 % compared to coatings obtained at a bias potential of -200 B. For sample no. 3, which has the best hardness indicators, we identified the highest adhesive strength of 49.54 N.

Coatings of TiSiN/WN system

The results of experimental studies of the structure and properties of multilayer TiSiN/WN coatings before and after annealing are given in [26, 27] and depicted in Figure 6.
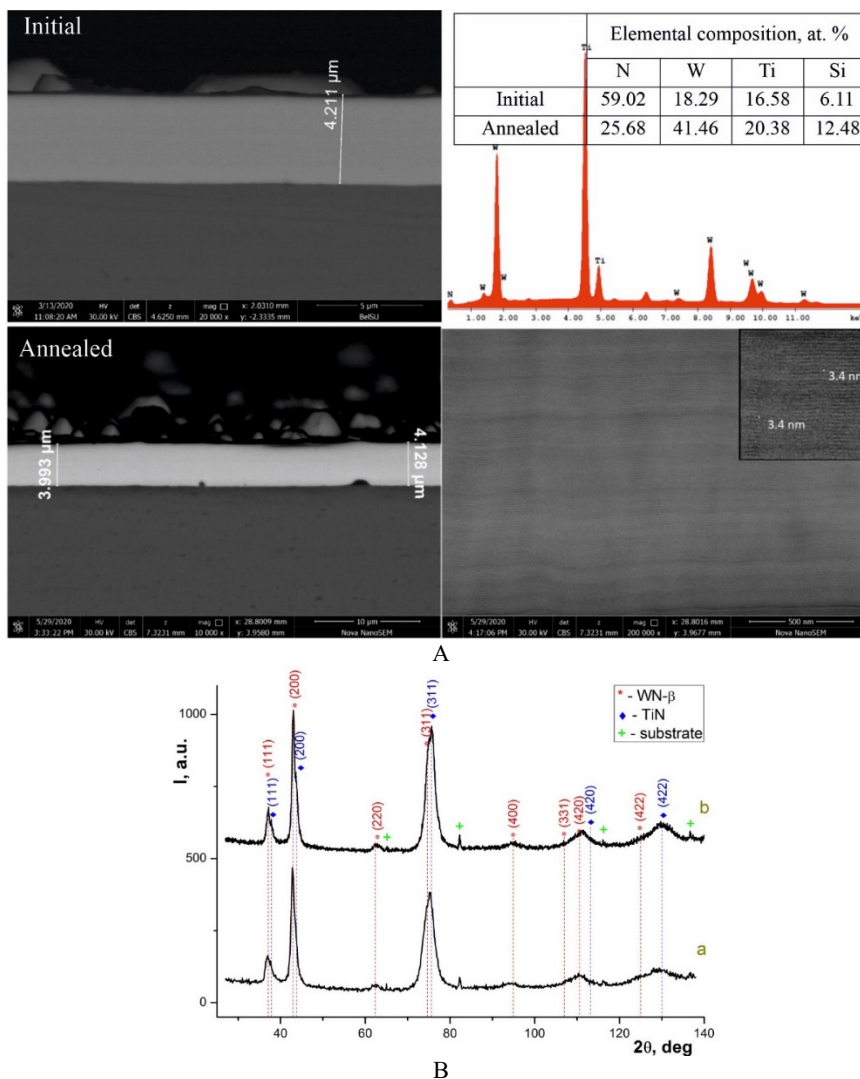
Figure 6. General research results of multilayer coatings TiSiN/WN: SEM images of the cross-sections with chemical analyses before and after annealing (a) XRD patterns before and after annealing (b)

It was established that all coatings have a relatively dense homogeneous structure (see Figure 6a). There are no cracks, pores, or other structural defects at the "substrate-coating" interface. According to the results of the quantitative analysis of the droplet phase, the average size of droplet formations in the coatings is approximately the same. Still, their number in the TiSiN/WN coating is reduced by two times compared to the WN/TiN coating due to the higher melting temperature of the TiSi system. After annealing, the surface of the coating's changes, while the main part, in the direction from the surface to the substrate, remains visually unchanged. Noticeable dimensional changes, in particular, the thickness of coatings decreases by 5 %.

It is seen that the heating intensified the diffusion processes that contributed to the changes in the atomic composition of the components (see Figure 6a). The titanium concentration increases from 16.58 to 20.38 at. % and tungsten concentration rise from 18.29 to 41.46 at. %. This may be due to the additional formation of solid solutions from TiSi and W atoms in the near-boundary region due to the diffusion processes and mixing. The silicon concentration increased approximately two times, from 6.11 to 12.48 at. %.

Experimental data show that nanosize multilayer TiSiN/WN coatings have a two-phase structure: cubic tungsten nitride WN-β and cubic titanium nitride TiN (see Figure 6b). The lattice parameter of WN-β is 0.4232 nm, the grain size is 8.2 nm, and the level of microdeformations is 6.3×10^{-3}. The intensity of the diffraction lines from WN-β and TiN indicates the predominant orientation (200) in the WN layers and (311) in the TiSiN layers. The titanium nitride lattice parameter is 0.4155 nm, the grain size is 9.0 nm, and the level of microdeformations is 1.35×10^{-2}. After annealing at 700 °C, the two-phase structure remained in the WN/TiSiN multilayer coatings. The lattice parameter of WN-β decreases the value of 0.4192 nm, the grain size increases to 12.6 nm, and the level of microdeformations decreases to 3.6×10^{-3}. The lattice parameter of TiN also reduces to 0.4124 nm, the grain size increases to 10.9 nm, and the level of microstrains decreases to 1.16×10^{-2}. The preferential orientation (200) remains unchanged.

It is obvious that annealing intensifies diffusion processes that cause changes in the atomic composition of elements. The Ti concentration increases from 18.29 to 20.08 at. %, and the W concentration rises from 18.29 to 41.46 at. %. Furthermore, the concentration of N decreases from 59 to 26 at. %, and Si increases almost two times (from 6.11 at. % to 12.48 at. %).

Diffraction lines containing silicon are absent in XRD patterns, which indicates the XRD amorphousness. The only change for the TiSiN/WN coating is that the reflections from WN-β are shifted to higher 2-theta values, which may be due to the annihilation of point defects (interstitial or substituted) often observed in vacuum-arc coatings obtained at high pressure of the working gas [28]. Annihilation should also affect the TiN lattice parameters. However, the diffusion effect of W in TiN can counteract the expected decrease in the lattice parameter, which is observed in this coating. During annealing, the phase state of the coatings did not change in principle, but it led to an increase in grain size and relaxation of internal stresses.

The indicators of the mechanical properties show that the hardness of the annealed coatings increased by 6-7 % (hardness values rise up to 33 GPa, elastic modulus grows up to 422 GPa, fracture deformation, and plastic deformation increses up to 0.078 and 0.202, respectively). In summary, annealing multilayer TiSiN/WN coatings at a moderate temperature partially eliminated structural and technological defects, improving mechanical characteristics.

**Coatings of TiSiN/TiZrN system**

Increasing the wear resistance of TiSiN-based coatings can be achieved by applying a multicomponent alternating layer, for instance, TiAlN or TiVN [10, 17]. Figure 7 shows the experimental results of the study of multilayer TiSiN/TiZrN coatings adopted from [29-31]. We used the targets made of alloys TiZr (element ratio is 75:25 at. %) and TiSi (elements ratio is 94:6 at. %). The technology used in target production is vacuum-arc remelting. As can be seen in Figure 7a, the surface of the coatings is not smooth, and the droplet fraction on the samples of all samples is present in a rather noticeable amount. In addition to drops, crater-pores are visible on the surface. The cross-sectional images clearly show the layered architecture and the diffusion zone formed at the "coating-substrate" interface. The multilayer combination has good planarity and the boundaries of layers of different compositions are well distinguished. According to chemical analysis, the content of silicon varied between 0.56 to 0.86 at. %, which is significantly lower than its content in the target (5 at. %). The likely reason for these decreases is backscattering.

According to XRD analysis (see Figure 7b), the two-phase structure with fcc crystal structure is formed. The TiZrN and TiN phases have reflections of the (111), (200), and (311) planes. The signal from the (111) planes is the most intense, which is the preferential orientation and can be considered a confirmation of the highest level of crystallinity. An increase in the multilayer period while maintaining the total thickness of the coating is accompanied by a similar decrease in the degree of crystallinity. As the multilayer period increases, splitting the (111) peak into components from the TiZrN and TiN phases becomes more noticeable. A similar pattern is also visible for the (311) peak. The average grain size ranges from 9.2 to 11.6 nm. In coatings deposited under different nitrogen pressures with the same other parameters, the grain size difference was only 0.2 nm, that is, only 2% on average. The architecture and structure of the coating are more significant influences on the grain size. Thus, an increase in the number of bilayers (in other words, a decrease in the multilayer period) from 90 to 180 and 360 leads to a consistent corresponding change in grain sizes along the chain: 11.6 nm (sample no. 4) - ≈10 nm (sample no. 1 and sample no. 2) - 9.2 nm (sample no. 3) and to increasing crystallinity (level of texture). During coatings deposition, compressive residual stresses are formed, increasing from -3.5 to -5.3 GPa

with grain size. The calculated dimensions of the lattice parameters differ little (the change range is between 0.4323 and 0.4354 nm); that is, the discrepancy does not exceed 1 %.

According to the data of photoelectron spectroscopy (see Figure 7c), the N 1s spectrum can be separated into two components, of which the main (high-intensity) peak at 395.3 eV can correspond to the energy of Si-N_x type bonds, probably in the Si_3N_4 compound. The low-energy peak at 395.5 eV may correspond to the Ti-N bond energy. The Ti 2p spectrum also splits into two components: the high binding energy at 397.2 eV corresponds to Ti-N type bonds, and the low binding energy at 396.3 eV corresponds to Zr-N bonds.
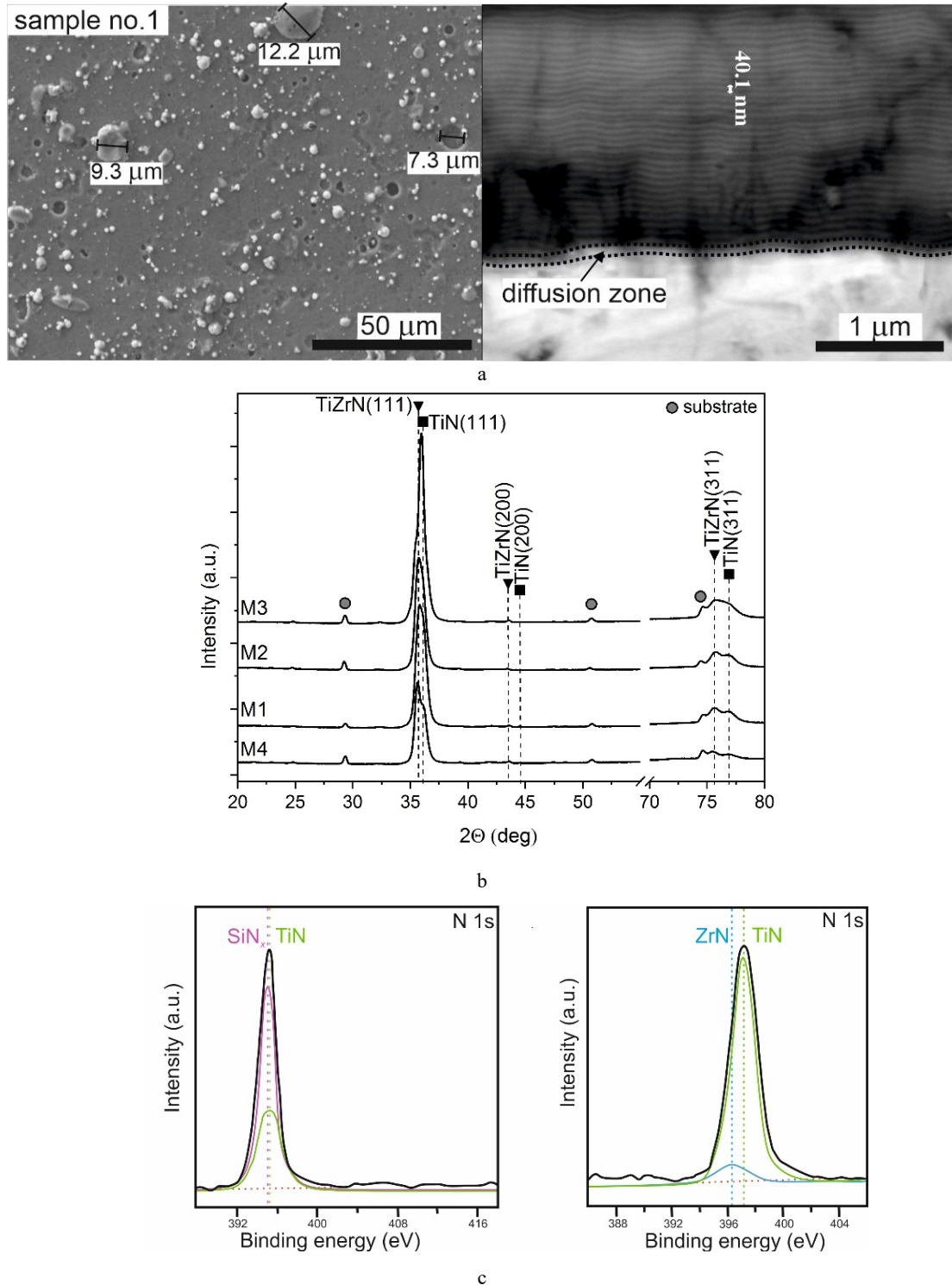
Figure 7. General research results of multilayer coatings TiSiN/TiZrN: typical SEM images of the surface and cross-section (a), XRD patterns (b), photoelectron spectroscopy spectra (c), results of sclerometric studies of the sample nos. 2 та 4 (the red line corresponds to the friction coefficient (COF) and the blue line corresponds to the acoustic emission (AE)) (d, e), SEM image of the scratch on the surface of sample no. 4 at different critical loads $L_{c1} - L_{c5}$ (f).

d   e

L_{c1} L_{c2} L_{c3} L_{c4} L_{c5}

f
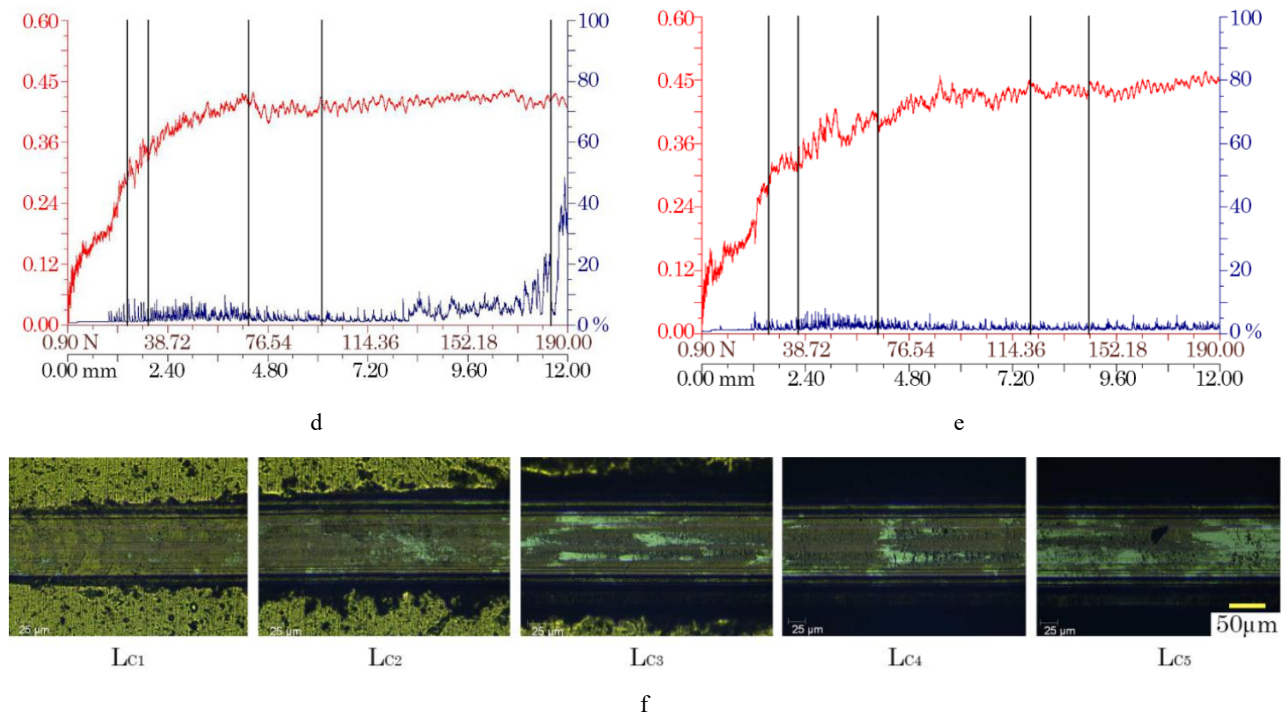
Figure 7. (continued) General research results of multilayer coatings TiSiN/TiZrN: typical SEM images of the surface and cross-section (a), XRD patterns (b), photoelectron spectroscopy spectra (c), results of sclerometric studies of the sample nos. 2 та 4 (the red line corresponds to the friction coefficient (COF) and the blue line corresponds to the acoustic emission (AE)) (d, e), SEM image of the scratch on the surface of sample no. 4 at different critical loads $L_{c1} - L_{c5}$ (f).

Compared to TiSiN or TiZrN films, multilayer TiZrN/TiSiN coatings have increased hardness, ranging from 24.5 GPa to 38.2 GPa. The trend of hardness increases with decreasing bilayer thickness, and the trend of hardness increases with decreasing bilayer thickness is evident. The coating with the thinnest multilayer period of 20 nm has the highest hardness of 38.2 GPa and modulus of elasticity of 430 GPa. Similar changes in friction coefficients and acoustic emission parameters were recorded for coatings obtained at different nitrogen pressures (see Figures 7d and 7e). When the load increases to ~55 N, the friction coefficients increase quite quickly and steadily to the level of ~0.5–0.52, after which it decreases slightly to the values of 0.46 - 0.47 and remains practically unchanged after that (not more than 0.48) to a maximum load of 190 N. During the entire period of loading and movement of the indenter on the coating surface, the level of acoustic emission (AE) is relatively low. The first pulses are recorded starting with a load of 15 N; the maximum level of AE is observed at loads of 25-45 N, although it does not exceed 5 %. Extreme AE peaks are not recorded, a characteristic feature of wear without brittle fracture. No peeling of the coating was recorded during scratching, indicating cohesive wear associated with plastic deformation and fatigue failure of the coating material. Scratches at different stages of loading indicate a smooth wear characteristic of plastic abrasion without clearly visible cracks (see Fig. 7f). Such wear is observed until the coating is completely worn to the substrate.

According to the wear testing results, multilayer TiSiN/TiZrN coatings wear by an abrasive mechanism. The intensity of wear of sample no. 3 (multilayer period is 20.4 nm) is twice as low as in sample no. 4 (the multilayer period is 85.9 nm). The coefficient of friction during the tests range from 0.79 to 0.82. The improvement of wear resistance of TiZrN/TiSiN nanocomposites is affected by their structural and phase features, in particular, multilayer period, concentration of Si atoms, the level of crystallinity (texture), and stress state.

Coatings of TiSiN/MoN system

Figure 8 shows experimental results for multilayer TiSiN/MoN coatings adopted from [32-35]. The vacuum-arc remelting method was applied to sinter the TiSi target. The compositions of the targets were $Ti_{94}Si_6$ and $Mo_{99.8}$. Microscopic analysis of the cross-section images of the coatings showed a reasonably high uniformity and low defectivity (see Figure 8a) of the obtained coatings by thickness. An increase in the bias potential causes more intense surface sputtering, while the thickness of the coating also decreases. It is shown that in the nitrogen pressure between 0.05 and 0.67 Pa, when the pressure increases, changes occur at the elemental level: The Si content decreases and the N and Mo/Ti ratios increase. At the phase level, changes mainly occur in molybdenum-based layers, where the transition $Mo \rightarrow \gamma\text{-}Mo_2N \rightarrow MoN$ occurs with increasing pressure. The highest hardness of 37.5 GPa is achieved in this case by forming $TiN/\gamma\text{-}Mo_2N$ layers with an isostructural crystal lattice. The use of high-temperature annealing (at a temperature of 1023 K) makes it possible to increase the hardness of the coatings obtained at a relatively low nitrogen pressure of 0.09 Pa when the formation of an additional solid Ti_5Si_3 phase is likely due to the low nitrogen content.
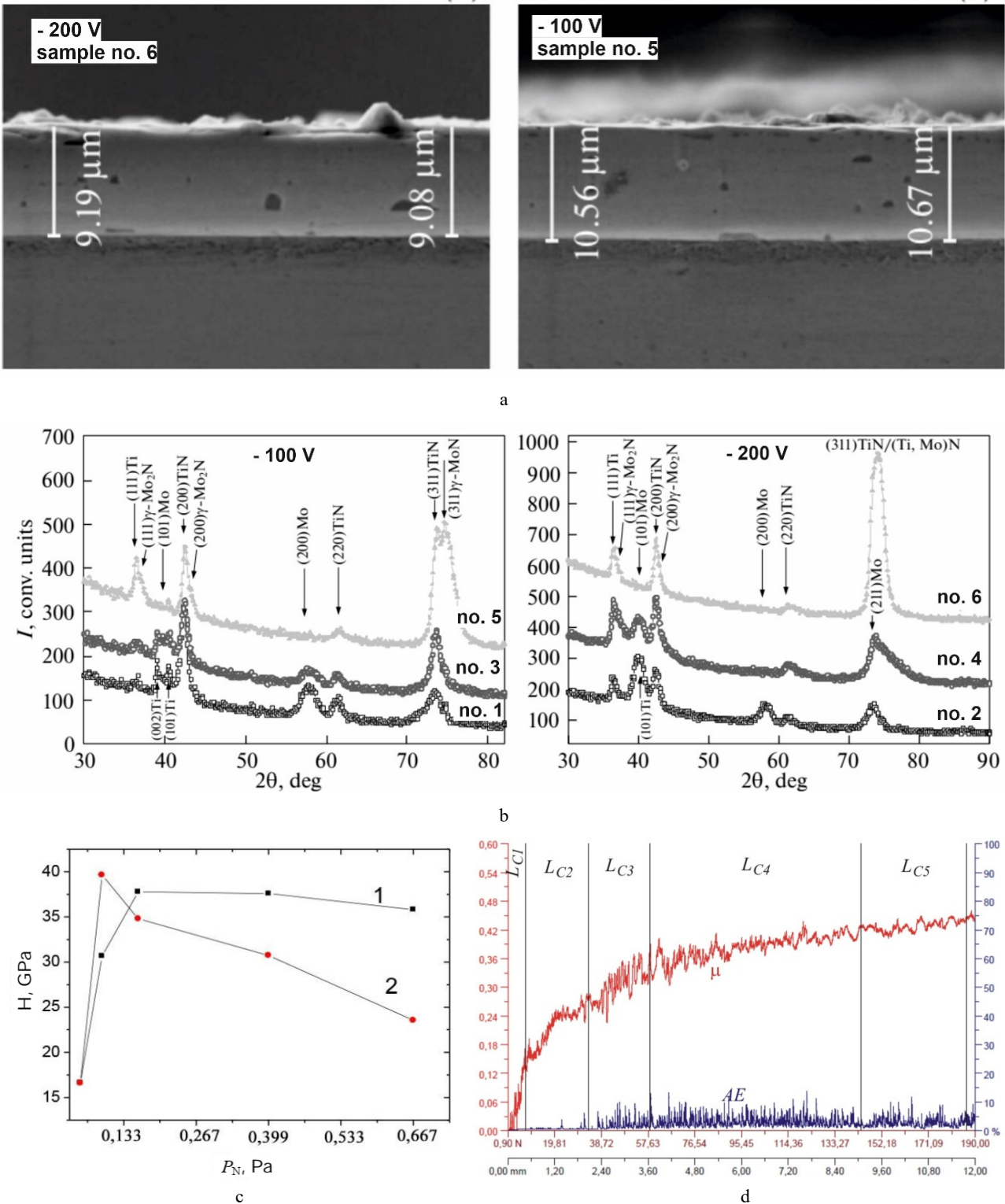
Figure 8. General research results of multilayer coatings TiSiN/MoN: cross-section SEM images (a), XRD patterns (b), dependence of hardness on the nitrogen partial pressure before (curve 1) and after annealing (curve 2) (c), results of sclerometric studies of the sample no. 4 (the red line corresponds to the friction coefficient (COF) and the blue line corresponds to the acoustic emission (AE)) (d).

The results of adhesion strength of multilayer TiSiN/MoN coatings are significantly higher compared to coatings based on TiAlSiN systems, TiZrSiN, and, TiHfSiN which were obtained by vacuum-arc deposition [36, 37]. Thus, the destruction of these coatings begins at an average load of 55-65 N, and in multilayer TiSiN/MoN coatings - at a load of 160-180 N. The measurement of hardness shows that the partial pressure of nitrogen, which affects the formation of the phase composition, also has a decisive effect on hardness. The dependence of hardness on pressure reaches maximum values of about 37.5 GPa in the pressure range between 0.16 to 0.4 Pa (see Figure 8c). From the point of view of structural engineering, this state corresponds to the presence of nitride phases TiN and γ-Mo$_2$N with an isostructural crystalline

lattice of the NaCl type in both layers. Annealing is accompanied by a decrease in the hardness of the coatings obtained in the pressure range of 0.15 to 0.7 Pa, which is associated with the characteristic growth of crystallites in the constituent phases. This is especially noticeable in the coatings obtained at a pressure of 0.7 Pa, when, according to phase analysis, the MoN phase with a hexagonal crystal lattice is formed in molybdenum-based layers. At the same time, annealing of the coatings obtained at a pressure of 0.7 Pa leads to a significant increase in hardness by more than 30 % (up to 40 GPa).

CONCLUSIONS

Based on the obtained research results, the main regularities of the formation of the composition and properties of multilayer coatings were analyzed. This allows for further development of more complex combined multilayer systems with improved physicomechanical and tribological properties, as well as improved biocompatibility.

Studies of multilayer coatings, which consist of a combination of nitride or carbide multielement layers and layers of binary nitrides of refractory or transition metals or layers of pure metals, allow combining within one coating the best properties of multielement and multilayer nitride or carbide coatings. Patterns of structure formation in multilayer and multielement coatings under certain deposition conditions, such as nitrogen atmosphere pressure, bias potential, and substrate temperature, can be used to conduct further fundamental scientific research to elucidate the mechanisms of structure formation of more complex coatings for which these mechanisms are unknown at the moment, or to create approaches to the formation of new types of coatings by varying deposition parameters, architecture, and elemental composition.

The main practical advantages of the proposed vacuum-arc coating deposition method are simplified control over the technological process, reduction of cost and energy consumption, good repeatability of results, and the possibility of relatively easy and fast industrial scaling of deposition technologies.

Modeling the structure and properties of multielement and multilayer coatings based on first-principle molecular dynamics can additionally explain and confirm assumptions about specific features of the formation of the structure and properties of multilayer and multicomponent coatings, which allows us to predict good prospects for its application in further fundamental and applied research more complex from the point of view of architecture coatings.

The results of the study of the properties presented in the review, in particular the structure, hardness, adhesive strength, and the effect of annealing, are the main characteristics that affect the formation of composite nano-sized multilayer coatings as highly efficient materials for multifunctional purpose. This opens new perspectives for the development of new combinations of structural materials and the optimization of their production technologies.

ORCID

Olga V. Maksakova, https://orcid.org/0000-0002-0646-6704; **Serhiy V. Lytovchenko,** https://orcid.org/0000-0002-3292-5468
Vyacheslav M. Beresnev, https://orcid.org/0000-0002-4623-3243; **Serhiy A. Klymenko,** https://orcid.org/0000-0003-1464-3771
Denis V. Horokh, https://orcid.org/0000-0002-6222-4574; **Bohdan O. Mazilin,** https://orcid.org/0000-0003-1576-0590
Maryna Yu. Kopiekina, https://orcid.org/0000-0002-5956-5503; **Klymenko S. An.,** https://orcid.org/0000-0002-7913-5519
Vadim V. Grudnitskii, https://orcid.org/0000-0003-3366-6776; **Oleg V. Glukhov,** https://orcid.org/0000-0003-2453-5504
Ruslan S. Galushkov, https://orcid.org/0000-0002-9105-9774

REFERENCES

[1] A.S. Manokhin, S.A. Klymenko, V.M. Beresnev, S.An. Klymenko, M.Yu. Kopeykina, V.O. Stolbovoy, and S.V. Litovchenko, *Cutting tools made of composites based on cubic boron nitride with a coating*, (Naukova dumka, Publishing House of the National Academy of Sciences of Ukraine, Kyiv, NVP, 2023).

[2] A.S. Manokhin, S.A. Klimenko, S.An. Klimenko, and V.M. Beresnev, "Promising Types of Coatings for PCBN Tools, J. Superhard Mater. **40**, 424–431 (2018). https://doi.org/10.3103/S1063457618060084

[3] A.S. Manokhin, S.A. Klimenko, V.M. Beresnev, et al., "Wear Rate of PcBN Cutting Tools Equipped with Nanolayered Protective Coatings," J. Superhard Mater. **42**, 423–431 (2020). https://doi.org/10.3103/S1063457620060076

[4] A. Cavaleiro, *Nanostructured Coatings*, (Springer-Verlag, 2006).

[5] A.D. Pogrebnjak, O.M. Ivasishin, and V.M. Beresnev, "Arc-evaporated nanoscale multilayer nitride-based coatings for protection against wear, corrosion, and oxidation," Uspehi Fiziki Metallov, **17**(1), 1–28 (2016). http://dx.doi.org/10.15407/ufm.17.01.001

[6] O.V. Maksakova. O.D. Pogrebnjak, and V.M. Beresnev, "Features of Investigations of Multilayer Nitride Coatings Based on Cr and Zr," Usp. Fiz. Met. **19**(1), 25-48 (2018). https://doi.org/10.15407/ufm.19.01.025

[7] W. Cheng, J. Wang, X. Ma, P. Liu, P.K. Liaw, and W. Li, "A review on microstructures and mechanical properties of protective nano-multilayered films or coatings," Journal of Materials Research and Technology, **27**, 2413-2442 (2023). https://doi.org/10.1016/j.jmrt.2023.10.012

[8] J.W. Du, L. Chen, J. Chen, and Y. Du, "Mechanical properties, thermal stability and oxidation resistance of TiN/CrN multilayer coatings," Vacuum, **179**, 109468 (2020). https://doi.org/10.1016/j.vacuum.2020.109468

[9]   S. Veprek, M.G.J. Veprek-Hejman, P. Kavrankova, and J. Prohazka, "Different approaches to superhard coatings and nanocomposites," Thin Solid Films, **476**(1), 1–29 (2005). https://doi.org/10.1016/j.tsf.2004.10.053

[10] Y.Y. Chang, H. Chang, L.J. Jhao, and C.C. Chuang, "Tribological and Mechanical Properties of Multilayered TiVN/TiSiN Coatings Synthesized by Cathodic Arc Evaporation," Surf. Coat. Technol. **350**, 1071–1079 (2018). https://doi.org/10.1016/j.surfcoat.2018.02.040

[11] M.S. Ahmed, Z.-F. Zhou, P. Munroe, L.K.Y. Li, and Z. Xie, "Control of the damage resistance of nanocomposite TiSiN coatings on steels: Roles of residual stress," Thin Solid Films. **519**(15), 5007-5012 (2011). https://doi.org/10.1016/j.tsf.2011.01.070

[12] J. Bull, "Failure mode maps in the thin film scratch adhesion test," Tribology International, **30**(7), 491-498 (1997). https://doi.org/10.1016/S0301-679X(97)00012-1

[13] I. Aksyonov, A.O. Andreev, V.A. Bilous, V.E. Strelnytskyi, and V.M. Khoroshikh, *Вакуумна дуга: джерела плазми, осадження покриттів, поверхневе модифікація*, [Vacuum arc: plasma sources, deposition of coatings, surface modification], (Naukova Dumka, Kyiv, 2012). (in Ukrainian)

[14] K Holmberg, *Matthews Coatings tribology: properties, mechanisms, techniques and applications in surface engineering*, *Tribology and interface engineering series*, vol. 56, (Elsivier, 2009).

[15] Q. Wan, B. Yang, H.D. Liu, J. Chen, and J. Zhang, "Microstructure and adhesion of MeN/TiSiN (Me = Ti, Cr, Zr, Mo, Nb_xAl_{1-x}) multilayered coatings deposited by cathodic arc ion plating," Applied Surface Science, **497**(15), 143602 (2019). https://doi.org/10.1016/j.apsusc.2019.143602

[16] S.-M. Yang, Y.-Y. Chang, D.-Y. Lin, D.-Y. Wang, and W. Wu, "Mechanical and tribological properties of multilayered TiSiN/CrN coatings synthesized by a cathodic arc deposition process," Surf. Coat. Technol. **202**(10), 2176–2181 (2008). https://doi.org/10.1016/j.surfcoat.2007.09.004

[17] C.L. Chang, W.C. Chen, P.C. Tsai, W.Y. Ho, and D.Y. Wang, "Characteristics and performance of TiSiN/TiAlN multilayers coating synthesized by cathodic arc plasma evaporation," Surf. Coatings Technol. **202**, 987-992 (2007). https://doi.org/10.1016/j.surfcoat.2007.06.024

[18] Y.X. Xu, L. Chen, F. Pei, Y. Du, "Structure and thermal properties of TiAlN/CrN multilayered coatings with various modulation ratios,' Surface and Coatings Technology. **304**, 512-518 (2016). https://doi.org/10.1016/j.surfcoat.2016.07.055

[19] A.S. Çam, T.O. Ergüder, G. Kaya, and F. Yıldız, "Improvement of structural/tribological properties and milling performances of tungsten carbide cutting tools by bilayer TiAlN/TiSiN and monolayer AlCrSiN ceramic films," Ceramics International, **48**(18), 26342-26350 (2022). https://doi.org/10.1016/j.ceramint.2022.05.318

[20] R. Pu, Z. Yu, X. Hao, J. Yan, Z. Han, J. Tan, L. Lu, *et al*., "Effect of Si content on microstructure, mechanical properties, and cutting performance of TiSiN/AlTiN dual-layer coating," J. Manuf. Process, **88**, 134 (2023). https://doi.org/10.1016/j.jmapro.2023.01.022

[21] O. Maksakova, V. Beresnev, S. Lytovchenko, and D. Kaynts, "A Comparative Study of Microstructure and Properties of TiZrN/NbN and TiSiN/NbN Nanolaminate Coatings," in: *Nanocomposite and Nanocrystalline Materials and Coatings. Advanced Structured Materials*, edited by A.D. Pogrebnjak, Y. Bing, and M. Sahul, vol. 214. (Springer, Singapore, 2024). pp. 163-180. https://doi.org/10.1007/978-981-97-2667-7_6

[22] D.V. Horokh, O.V. Maksakova, S.A. Klimenko, S.V. Lytovchenko, V.M. Beresnev, and O.V. Glukhov, "The Influence of the bias potential answorking gas pressure on the properties of the ion-plasma multilayer coating TiSiN/NbN," Journal of Superhard Materials, **44**(6), 413–420 (2022). https://doi.org/10.3103/S1063457622060041

[23] V.M. Beresnev, S.V. Lytovchenko, O.V. Maksakova, A.D. Pogrebnjak, D.V. Horokh, and U.S. Shvets, "Microstructure and High-hardness Effect in TiSiN/NbN Nanomultilayers: Experimental Research," in: *2021 IEEE 11th International Conference Nanomaterials: Applications & Properties (NAP)*, (Odessa, Ukraine, 2021), pp. 1-4, https://doi.org/10.1109/NAP51885.2021.9568502

[24] V.M. Beresnev, O.V. Maksakova, S.V. Lytovchenko, S.A. Klymenko, D.V. Horokh, A.S. Manohin, B.O. Mazilin, *et al*., "Correlating Deposition Parameters with Structure and Properties of Nanoscale Multilayer (TiSi)N/CrN Coatings," East European Journal of Physics, (2), 112-117 (2022). https://doi.org/10.26565/2312-4334-2022-2-14

[25] D.V. Horokh, O.V. Maksakova, V.M. Beresnev, S.V. Lytovchenko, S.A. Klimenko, V.V. Grudnitsky, I.V. Doshchechkina, et al., "Influence of annealing on the physical and mechanical properties of (TiSi)N/CrN multilayer coatings produced by cathodic arc physical vapour deposition, High Temperature Material Processes, **27**(4), 1-14 (2023). https://doi.org/10.1615/HighTempMatProc.2022046618

[26] M. Beresnev, S.V. Lytovchenko, O.V. Maksakova, A.D. Pogrebnjak, V.A. Stolbovoy, S.A. Klymenko, and L.G. Khomenko, "Microstructure and high-hardness effect in WN-based coatings modified with TiN and (TiSi)N nanolayers before and after heat treatment: experimental investigation," High Temperature Material Processes, **25**(4), 61–72 (2021). https://doi.org/10.1615/HighTempMatProc.2021041565

[27] M. Sahul, B. Bočáková, K. Smyrnova, M. Haršáni, M. Sahul, M. Truchly, M. Kusý, et al., "The Influence Of Multilayer Architecture On The Structure And Mechanical Properties Of WN_X/TiSN Coatings In Comparison With WN_X and TiSiN Single Layers," Journal of Physics Conference Series, **2413**(1), 012013 (2022). https://doi.org/10.1088/1742-6596/2413/1/012013

[28] L. Rogström, N. Ghafoor, J. Schroeder, N. Schell, J. Birch, M. Ahlgren, and M. Odén, "Thermal Stability of Wurtzite $Zr_{1-x}Al_xN$ Coatings Studied by In Situ High-Energy X-Ray Diffraction during Annealing," J. App. Phys. **118**, 035309 (2015). https://doi.org/10.1063/1.4927156

[29] V.M. Beresnev, S.V. Lytovchenko, D.V. Horokh, B.O. Mazilin, V.A. Stolbovoy, I.N. Kolodiy, D.A. Kolesnikov, *et al*., "Tribotechnical properties of (TiZr)N/(TiSi)N multilayer coatings with nanometer thickness," Journal of Nano- and Electronic Physics, **11**(5), 05037 (2019). https://doi.org/10.21272/jnep.11(5).05037

[30] V.M. Beresnev, S.V. Lytovchenko, B.O. Mazilin, D.V. Horokh, V.A. Stolbovoy, D.A. Kolesnikov, I.V. Kolodiy, *et al*., "Adhesion strength of TiZrN/TiSiN nanocomposite coatings on a steel substrate with transition layer," Journal of Nano- and Electronic Physics, **12**(4), 04030 (2020). https://doi.org/10.21272/jnep.12(4).04030

[31] O.V. Maksakova, S. Zhanyssov, S.V. Plotnikov, P. Konarski, P. Budzynski, A.D. Pogrebnjak, V.M. Beresnev, *et al*., "Microstructure and tribomechanical properties of multilayer TiZrN/TiSiN composite coatings with nanoscale architecture by cathodic-arc evaporation," J. Matirial. Sci. **56**, 5067–5081 (2021). https://doi.org/10.1007/s10853-020-05606-2

[32] V.M. Beresnev, O.V. Sobol, A.A. Meylekhov, A.A. Postelnik, V.Yu. Novikov, Y.S. Kolesnikov, V.A. Stolbovoy, *et al*., "Effect of Pressure of Nitrogen Atmosphere During the Vacuum Arc Deposition of Multiperiod Coatings (Ti, Si)N/MoN on their Structure and Properties," J. Nano- Electron. Phys. **8**(4), 04023 (2016). https://doi.org/10.21272/jnep.8(4(1)).04023

[33] V.M. Beresnev, U.S. Nyemchenko, P.O. Srebniuk, S.V. Lytovchenko, and O.V. Sobol′, "Study of influence physical and technological parameters of deposition on the structure, physical and mechanical properties of vacuum-arc coatings (Mo + Ti6%Si)N," in: *Proceegings of 6-th International Conference Nanomaterials: Applications and Properties*, **5**(1), 01FNC08 (2016). https://doi.org/10.1109/NAP.2016.7757226

[34] O.V. Sobol, A.A. Meylehov, A.A. Postelnyk, S.V. Litovchenko, P.A. Srebniuk, U.S. Nyemchenko, and V.M. Beresnev, "Effect of Deposition Process Parameters and High-temperature annealing on the structure and proprerties of (TiSi)MoN vacuum-arc coatings," in: *Proceegings of 2017 IEEE 7-th International Conference Nanomaterials: Applications and Properties (NAP-2017)*, (Zatoka, 2017). https://doi.org/10.1109/NAP.2017.8190211

[35] V.M. Beresnev, S.A. Klimenko, O.V. Sobol, S.V. Litovchenko, A.D. Pogrebnjak, P.A. Srebnyuk, D.A. Kolesnikov, *et al*., "Influence of the High-temperature annealing on the structure and mechanical properties of vacuum-arc coatings from (Mo/Ti, 6 wt.% Si)N," J. Superhard Materials, **39**(3), 172-177 (2017). https://doi.org/10.3103/S1063457617030042

[36] S. Carvalho, L. Rebouta, E. Ribeiro, F. Vaz, C.J. Tavares, E. Alves, N.P. Barradas, *et al*., "Structural evolution of Ti–Al–Si–N nanocomposite coatings," Vacuum, **83**(10), 1206–1212 (2009). https://doi.org/10.1016/j.vacuum.2009.03.009

[37] V.M. Beresnev, S.A. Klimenko, I.N. Toryanik, A.D. Pogrebnjak, O.V. Sobol, P.V. Turbin, and S.S. Grankin, "Superhard coatings of the (Zr–Ti–Si)N and (Ti–Hf–Si)N systems produced by vacuum–arc deposition from a separated flow," J. Superhard Mater. **36**(1), 29–34 (2014). https://doi.org/10.3103/S1063457614010055

ОГЛЯД ВАКУУМНО-ДУГОВИХ БАГАТОШАРОВИХ ПОКРИТТІВ З ВИСОКИМИ ХАРАКТЕРИСТИКАМИ МІЦНОСТІ ТА АДГЕЗІЙНИМИ ВЛАСТИВОСТЯМИ

О.В. Максакова[a,b], С.В. Литовченко[a], В.М. Береснєв[a], С.А. Клименко[c], Д.В. Горох[a], Б.О. Мазілін[a], М.Ю. Копєйкіна[c], С.Ан. Клименко[c], В.В. Грудницький[d], О.В. Глухов[e], Р.С. Галушков[a]

[a]*Харківський національный університет імені В.Н. Каразіна, майдан Свободи 4, 61022, м. Харків, Україна*
[b]*Інститут матеріалознавства, Словацький технологічний університет у Братиславі,*
25, вул. Яна Ботту , 917 24, Трнава, Словаччина
[c]*Інститут надтвердих матеріалів імені В.Н. Бакуля НАН України, вул. Автозаводська, 2, м. Київ, Україна*
[d]*Національный науковий центр «Харківський фізико-технічний інститут»,*
вул. Академічна, 1, 61108, м. Харків, Україна
[e]*Харківський національний університет радіоелектроніки, пр. Науки, 14, 61166, м. Харків, Україна*

На прикладі системи покриттів TiSiN/MeN (Me = Cr, Nb, W, Mo, TiZr) проаналізовано результати створення багатошарових покриттів з наношарами різного функціонального призначення, які потребують системного підходу до розуміння ролі обраних матеріалів, умов росту, мікроструктури та необхідних властивостей. Нанорозмірні межі зерен, когерентні міжшарові границі та зміни стовпчастої морфології на мікрорівні суттєво змінюють фізико-механічні властивості покриттів. Для всіх покриттів спостерігається покращення механічних характеристик (твердість, модуль пружності) за рахунок утворення нанорозмірної фази (яка додатково перешкоджає руху дислокацій разом з нанокомпозитом TiSiN). Крім того, зафіксована невідповідність кристалічних граток окремих шарів ефективно сприяє зміцненню внаслідок утворення змінних полів напружень і пружних деформацій. Дослідженнями визначено оптимальні умови формування покриттів у широкому діапазоні тиску рекційного газу (азоту) та потенціалу зміщення, що також дозволило встановити фактори структурних змін та експлуатаційні характеристики, які будуть оптимальними для їх промислового використання.

Ключові слова: *вакуумно-дугове осадження; багатошарові покриття; TiSiN; потенціал зміщення; твердість; фазовий стан; відпал*